

COLD GASS, an IRAM Legacy Survey of Molecular Gas in Massive Galaxies: III. Comparison with semi-analytic models of galaxy formation

Guinevere Kauffmann^{1*}, Cheng Li², Jian Fu^{1,2}, Amélie Saintonge³, Barbara Catinella¹, Linda J. Tacconi³, Carsten Kramer⁴, Reinhard Genzel³, Sean Moran⁵, David Schiminovich⁶

¹*Max-Planck Institut für Astrophysik, 85741 Garching, Germany*

²*Max-Planck-Institut Partner Group, Shanghai Astronomical Observatory*

³*Max-Planck Institut für extraterrestrische Physik, 85741 Garching, Germany*

⁴*Instituto Radioastronomía Milimétrica, Av. Divina Pastora 7, Nucleo Central, 18012 Granada, Spain*

⁵*Johns Hopkins University, Baltimore, Maryland 21218, USA*

⁶*Department of Astronomy, Columbia University, New York, NY 10027, USA*

11 April 2018

ABSTRACT

We compare the semi-analytic models of galaxy formation of Fu et al. (2010), which track the evolution of the radial profiles of atomic and molecular gas in galaxies, with gas fraction scaling relations derived from a stellar mass-limited sample of 299 galaxies from the COLD GASS survey. These galaxies have measurements of the CO(1-0) line from the IRAM 30-m telescope and the HI line from Arecibo, as well as measurements of star formation rates, stellar masses, galaxy sizes and concentration parameters from GALEX+SDSS photometry. The models provides a good description of how condensed baryons in star-forming galaxies are partitioned into atomic and molecular gas and stars as a function of galaxy stellar mass and stellar surface density. The models do not reproduce the observed tight relation between stellar surface mass density and bulge-to-disk ratio in these galaxies. The current implementation of “radio-mode feedback” in the models produces trends that disagree strongly with the data. In the models, gas cooling shuts down in nearly all galaxies in dark matter halos above a mass of $\sim 10^{12} M_{\odot}$. As a result, stellar mass is the observable that best predicts whether a galaxy has little or no neutral gas, i.e. whether a galaxy has been quenched. In contrast, our data show that quenching is largely *independent* of stellar mass. Instead, there are clear thresholds in bulge-to-disk ratio and in stellar surface density that demarcate the location of quenched galaxies in our chosen parameter space. We speculate that the disagreement between the models and the observations may be resolved if radial transport of gas from the outer disk is included as an additional bulge-formation mechanism in the models. In addition, we propose that processes associated with bulge formation play a key role in depleting the neutral gas in galaxies and that gas accretion is suppressed in a significant fraction of galaxies following the formation of the bulge, even in dark matter halos of low mass.

Key words: galaxies: fundamental parameters – galaxies: evolution – galaxies: ISM – radio lines: galaxies – surveys

1 INTRODUCTION

An important goal in modern galaxy formation is an improved understanding of the physical processes that regulate the rate at which stars form in galaxies. These processes include the cooling and accretion of gas within dark matter

halos, the transformation of the accreted gas into molecular clouds and stars, and the effects of “feedback” from massive stars and accreting black holes on the gas in and around galaxies.

The Lambda-Cold Dark Matter model provides detailed predictions for how dark matter halos assemble over time. Within these halos, gas will cool and settle into a rotationally-supported disk. One hotly debated issue is the

* E-mail: gamk@mpa-garching.mpg.de

degree to which gas loses angular momentum to the surrounding dark matter during this process. In many “semi-analytic” models, the angular momentum of the gas is assumed to be conserved. This produces a size-circular velocity relation for galactic disks that is in good agreement with observations (Mo, Mao & White 1998). More detailed numerical hydrodynamical simulations of disk galaxy formation in a Λ CDM universe demonstrate, however, that the amount of angular momentum that is lost during the collapse of the dark matter halo depends sensitively on how feedback processes are included in the models (Navarro & Steinmetz 1997; Governato et al 2004, 2007). In many simulations, the disks form early and are too compact. The resulting star formation timescales are then too short to be consistent with observations (e.g. Oser et al 2010).

Another important unsolved problem is to understand why galaxies divide into two distinct “families” – those with ongoing active star formation, and those where star formation has been quenched (Strateva et al 2001; Kauffmann et al 2003b; Baldry et al 2004). It has now become clear that these distinctions existed already at redshifts as high as 2.5 (Williams et al 2010; Wuyts et al 2011), when cold gas accretion rates in almost all dark matter halos are predicted to be very high.

Many recent theoretical galaxy formation models that aim to reproduce the statistical properties of the massive galaxy population (e.g. Croton et al 2006; Bower et al 2006; Cattaneo et al 2006; De Lucia & Blaizot 2007; Somerville et al 2008; Guo et al 2011; Lu et al 2011) invoke star-formation quenching mechanisms that set in at a characteristic dark matter halo mass. The characteristic mass is associated with the transition between the regime where gas cooling times are short compared to the dynamical time of the dark matter halo and gas accretes in the form cold, condensed clouds, and the regime where cooling times are long and gas accretes from a corona of gas that is in virial equilibrium with the surrounding halo.

One might ask *why* lowered rates of star formation in galaxies should be linked with this transition. One argument that is often used is that relativistic jets, generated when gas accretes onto black holes, heat the surrounding hot gas and prevent it from forming stars (see, for example, Croton et al. 2006). The conditions under which black holes produce jets are not well understood. There is clear observational evidence that radio-emitting jets play a role in regulating the cooling of gas in nearby galaxy clusters (see McNamara & Nulsen 2007 for a recent review). Theoreticians have thus made an “ansatz” that jets from radio-loud AGN will prevent gas from cooling and forming stars in *all* dark matter halos that are predicted to contain a hot gas atmosphere. The characteristic halo mass threshold that separates star-forming and quiescent galaxies is the main factor that determines how massive galaxies evolve in current models, so it is clearly important to test the existence of such a threshold using real observations.

We note that accretion and quenching processes affect the *gas components* of galaxies. The most direct empirical constraints on how they operate thus come from observations of the gas in galaxies. This has been the primary motivation for the Galex Arecibo SDSS survey (GASS), as well as the CO Legacy Database for GASS (COLD GASS), which are measuring the atomic and molecular gas contents of an

unbiased sample of several hundred galaxies with redshifts between 0.025 and 0.05, and with stellar masses in the range $10^{10} < M_* < 10^{11.5} M_\odot$. In both surveys, the strategy is to observe each galaxy until the HI/CO lines are detected, or until upper limits in the ratio of atomic and molecular gas mass to stellar mass of ~ 0.015 reached. The aim of the program is to carry out a census of the condensed baryons in galaxies in the local Universe, to study scaling relations between the gas and stellar properties of these galaxies, and to understand gas accretion and quenching in galaxies.

Details of the GASS and COLD GASS survey designs, as well as target selection and observing procedures are given in Catinella et al (2010) and Saintonge et al (2011a). These two papers also presented relations between the HI and H₂ mass fractions of galaxies (defined as M_{HI}/M_* and M_{H_2}/M_*) and global galaxy parameters such as stellar mass M_* , stellar mass surface density μ_* , galaxy bulge-to-disc ratio (as parameterized by the concentration index C of the r -band light), and specific star formation rate SFR/M_* (see also Schiminovich et al 2010). The two surveys uncovered sharp thresholds in μ_* and C below which all galaxies have a measurable cold gas component, but above which the detection rate of the CO and HI lines drops suddenly, suggesting that “quenching processes” have occurred in these systems.

In this paper, we compare the observed gas fraction relations from the COLD GASS survey with predictions from the semi-analytic models of Fu et al (2010; hereafter F10), which track the formation of molecular gas in disk galaxies. The F10 models are based on the L-galaxies semi-analytic code, described in detail in Croton et al (2006) and updated in De Lucia & Blaizot (2007).

The models are currently being configured to operate on the latest update of the L-galaxies code by Guo et al. (2011); the comparison in this paper will be restricted to the version of the models in the published F10 paper. The main new aspect of these models is that galactic discs are represented by a series of concentric rings in order to track the evolution in the gas and stellar surface density profiles of galaxies over cosmic time. Two simple prescriptions for molecular gas formation processes are included: one is based on the analytic calculations by Krumholz, McKee & Tumlinson (2009; hereafter KMT), and the other is a prescription where the H₂ fraction is determined by the pressure of the interstellar medium (Blitz & Rosolowsky 2006, hereafter BR), with an implementation similar to that in Obreschkow et al. (2009). The free parameters of the models that regulate the rate at which gas is turned into stars and the efficiency with which supernovae reheat gas as a function of halo mass have been tuned to reproduce a number of key observables, including the observed present-day galaxy luminosity function, the gas-phase mass-metallicity relation, and the mean HI gas fraction as a function of B-band luminosity (see De Lucia, Kauffmann & White (2004) for a more detailed discussion).

There have been a number of other cosmological models that follow the formation of molecular gas in disks. Lagos et al (2011) have developed semi-analytic models that track molecular gas formation in cosmological simulations of galaxy formation, but these models do not predict the detailed radial profiles of galaxies as in F10. Robertson & Kravtsov (2008) and Dutton et al (2010) model the radial profiles of the gas and stars in galaxies, but their models

are not embedded within full cosmological N-body simulations. Gnedin et al (2009) have carried out very high resolution cosmological simulations of molecular gas formation that include radiative transfer and detailed treatment of the chemistry, but their box sizes are too small to make statistical predictions.

The F10 paper demonstrated that their models could fit the radial HI, H₂, stellar mass and SFR profiles of spiral galaxies from the THINGS/HERACLES surveys. In this paper, we investigate whether the models also yield correct gas fraction scaling relations and distribution functions. As will be seen, it is useful to break this analysis into two distinct parts: 1) comparison between models and observations of the distribution of gas fractions in the population of galaxies with detectable gas, 2) comparison of how *absence of gas*, which we refer to as “quenching”, is manifested as a function of observable quantities such as stellar mass, stellar surface density, and bulge-to-disk ratio. As we will show, such a comparison elucidates those aspects of the models which work well, and those that fail. Throughout this paper, we have assumed a cosmology with $\Omega = 0.3$, $\Lambda = 0.7$ and $H_0 = 70 \text{ km s}^{-1} \text{ Mpc}^{-1}$ to derive our observational quantities. The cosmology assumed for the F10 model is a Λ CDM models with $\Omega = 0.25$, $\Lambda = 0.75$, $H_0 = 73 \text{ km s}^{-1} \text{ Mpc}^{-1}$ and $\sigma_8 = 0.9$.

2 GENERATING COMPARISON SAMPLES FROM THE SIMULATIONS

The semi-analytic models used in this paper are nearly identical to those described in detail in F10. We have made only one small change. The free parameters in the F10 models were chosen so that reasonable fits to a variety of observables could be obtained. These observables included the H₂ mass function of Keres et al (2003) derived using galaxies drawn from the FCRAO Extragalactic CO Survey (Young et al 1995). These authors adopted a CO-to-H₂ conversion factor that was a factor of 1.5 times larger than the one adopted by Saintonge et al (2011a).¹ To bring the simulations back into agreement with the H₂ data using the conversion factor adopted by Saintonge et al, we simply increase the supernova reheating rate (given by the parameter ϵ_{disc}) in Table 1 of F10 by a similar factor ($\epsilon_{disc} = 5$ instead of 3.5). We note that changing ϵ_{disc} simply shifts the amplitude of the gas mass fraction scaling relations up or down. It does not change the predicted slope or scatter in these relations. We also note that the H₂ mass function derived from the COLD GASS data for galaxies with $\log M_* > 10^{10} M_\odot$ agrees well with that of Keres et al (2003) at the high mass end, once the same CO-to-H₂ conversion factor is adopted (Fu et al 2012, in preparation).

The observational sample is an update to that described in Saintonge et al 2011(a), consisting of 299 galaxies with CO(1-0) line observations with the IRAM 30 m telescope. HI line measurements from the GASS survey (Catinella et al 2010) are available for 270 out of the 299 galaxies. Because the observational sample is selected only by stellar mass, it is easy to compare simulation results directly with the

data. There are only two observational selection issues that require careful treatment:

(i) In both the GASS and COLD GASS surveys, targets are selected so that the resulting stellar mass distribution is approximately flat. This was done in order to be able to compute gas fractions in different stellar mass bins with roughly the same errors. The sampling must be taken into account when we look at gas fraction distributions as a function of parameters other than stellar mass. In this paper, we adopt two approaches: a) We either weight each galaxy in the sample by the inverse of $f(M_*)$, where $f(M_*)$ is the “sampling rate function” required to transform the true stellar mass distribution to a flat one, b) We apply the sampling rate function $f(M_*)$ to the simulated galaxies to create “mock catalogue” with flat stellar mass distributions that can be compared directly with the data.

(ii) It is important to take account of the detection limits of the survey when comparing model galaxies with the data. This is illustrated in the top panels of Figure 1, where we plot $M(\text{HI})/M_*$ (left) and $M(\text{H}_2)/M_*$ (right) as a function of stellar mass for 299 galaxies that have been observed in CO as of July 2011 (270 of these have HI observations from the GASS survey). Galaxies where the HI or CO line was detected (see Catinella et al 2010 and Saintonge et al 2011a for details about line detection procedures) are plotted in blue. Galaxies without detections are plotted in red at the positions of their 5σ upper limits in $M(\text{HI})/M_*$ or $M(\text{H}_2)/M_*$.

To a very close approximation, the HI mass fraction limit $\log [M(\text{HI})/M_*]_{lim}$ is -1.82 (corresponding to a HI mass fraction limit 0.015) for galaxies with $\log M_* > 10.3$. For galaxies with $10 < \log M_* < 10.3$, $\log [M(\text{HI})/M_*]_{lim} = -1.066 \log M_* + 9.16$.

The CO line detection limits are somewhat more complicated. As discussed in Saintonge et al (2011a), the integration times are set so that $\log [M(\text{H}_2)/M_*]_{lim} = -1.82$ for galaxies with $\log M_* > 10.6$. For lower mass galaxies, integration times are nominally set to reach a fixed r.m.s. of around 1.1 mK per 20 km/s wide channel, but the actual value fluctuated according to weather conditions at the time of observation. Therefore, when creating our mock catalogues from the simulations, we simply impose a distribution of upper limits similar to that seen in the top right panel of Figure 1. We take $[M(\text{H}_2)/M_*]_{lim,max}$, the *maximum* possible value of the H₂ mass fraction limit, as $\log [M(\text{H}_2)/M_*]_{lim,max} = -1.72$ if $\log M_* > 10.6$, and $\log [M(\text{H}_2)/M_*]_{lim,max} = 8.78 - \log M_*$ if $\log M_* < 10.6$. The H₂ mass fraction limit that we adopt is randomly distributed between the maximum value and a minimum value that is 0.35 dex smaller.

In this way, we are able to classify galaxies in the simulations as HI/CO “detections” or “non-detections” and compare properties such as stellar masses, stellar surface densities, specific star formation rates and concentration indices with those of the real galaxies in our survey. We note that stellar masses and star formation rates are standard outputs of semi-analytic models. Because the F10 models are able to track radial profiles of the gas and the stars in galaxies, they are also able to predict stellar surface mass densities, which are defined as $0.5M_*/(\pi R_{50}^2)$, where R_{50} is the radius containing half the stellar mass of the galaxy.

¹ $\alpha_{\text{CO}} = 3.2 M_\odot (\text{K km s}^{-1} \text{ pc}^2)^{-1}$, which does not include a correction for the presence of helium.

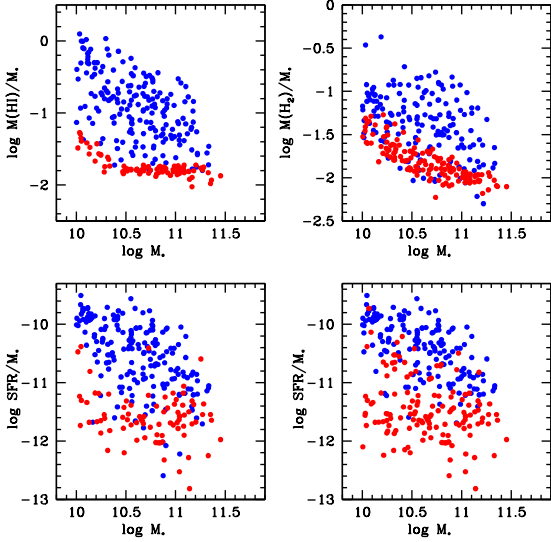


Figure 1. In the left panels, HI mass fraction ($\log M(\text{HI})/M_*$) and specific star formation rate ($\log \text{SFR}/M_*$) are plotted as a function of the $\log M_*$. Blue points denote galaxies with HI line detections. Red points denote galaxies where HI was not detected. In the right panels, H_2 mass fraction ($\log M(\text{H}_2)/M_*$) and specific star formation rate ($\log \text{SFR}/M_*$) are plotted as a function of the $\log M_*$. Blue points denote galaxies with CO line detections. Red points denote galaxies where CO was not detected.

In semi-analytic models, bulges form either as a result of a merger between two galaxies, or as a consequence of instabilities that set in when disks reach a certain critical threshold density. In the models, the total mass of the bulge is more reliably predicted than its size. As shown in Figure 1 of Weinmann et al (2009), there is a tight correlation between the concentration index C (defined as the ratio of the radii containing 90% and 50% of the r -band light) and galaxy bulge-to-disk ratio derived using 2-dimensional decomposition codes (Gadotti 2009). We have therefore elected to transform the bulge-to-disk ratios predicted by the models to concentration indices using a fit to this relation: $C = 1.8 + 2.14B/T$.

3 RESULTS

In the analysis presented in this paper, we will attempt to answer two questions:

- (i) Can the simple disk formation models described in the F10 paper explain observed gas fraction scaling relations for galaxies with gas?
- (ii) Does the transition between the population of galaxies with gas and the population without gas occur in the same way in the models and in the data?

We have chosen the gas fraction detection threshold of our two surveys as the nominal division between the population of galaxies we will henceforth refer to as “active” and the population that we will call “quenched”. Note that it is possible that some fraction of galaxies classified as “active” are actually losing their gas and evolving into quenched

systems. Conversely, some fraction of galaxies classified as “quenched” may have simply run out of gas just prior to the next accretion episode. Such galaxies may be thought of as “transition” systems.

In the bottom panels of Figure 1, we plot specific star formation rate versus stellar mass for the galaxies in our sample. In the left panel, galaxies with HI detections are colour-coded blue and those where the HI line was not detected are colour-coded red. In the right panel, we do the same thing according to whether the CO line was detected or not. As can be seen, galaxies with $\log \text{SFR}/M_* < -11$ are not usually detected in HI and almost never in CO. This means that there is a rather clean distinction between “active” and “quenched” galaxies that applies to both gas fraction and specific star formation rate for the majority of galaxies in our sample. In section 3.2.2, we return to the issue of whether we can identify a sub-population of galaxies that is in the *process* of being quenched.

3.1 Gas scaling relations for the active population

In Figures 2 and 3 we compare the mean HI and H_2 gas fractions as a function of M_* , μ_* , C and SFR/M_* for data and for models. The reader is referred to Catinella et al (2010) and Saintonge et al (2011a) for details on how HI and CO line fluxes are transformed into HI and H_2 masses. We note that we have adopted a constant Galactic conversion factor $\alpha_{\text{CO}} = 3.2M_\odot (\text{K km s}^{-1} \text{ pc}^2)^{-1}$, which does not include a correction for the presence of helium. A constant conversion factor should be a reasonable approximation for the galaxies in our survey, which all have stellar masses greater than $10^{10}M_\odot$ and gas-phase metallicities near solar (Saintonge et al 2011b).

In Figures 2 and 3, the blue points show the mean values of $M(\text{HI})/M_*$ and $M(\text{H}_2)/M_*$ calculated using the galaxies with HI and CO line detections. Error bars are calculated using bootstrap resampling. The red and black curves indicate the mean values calculated from the model galaxies that are classified as detections (see section 2). The black curves show results from the F10 model that uses the KMT prescription for the conversion of atomic to molecular gas. The red curves show results from the F10 model that uses the BR pressure-based prescription. We note that there are many more simulated galaxies than observed galaxies. In generating the curves, we have ordered the galaxies by increasing M_* , μ_* , C and SFR/M_* and computed means for bins of 70 galaxies.

Figures 2 and 3 show that the models reproduce the observed scalings between mean HI/ H_2 mass fraction and galaxy stellar mass, surface mass density and concentration quite well. The differences between the HI mass fractions predicted by the KMT and BR prescriptions are small. Given the systematic uncertainties in the calibration of the BR prescription, the fact that the KMT prescription is based on simple analytic calculations, the fact that our semi-analytic disc formation models are extremely idealized, and the fact that the model free parameters were not tuned to fit the COLD GASS scaling relations, we find it remarkable how well these results agree with the data.

The relation between H_2 mass fraction and specific star formation is *shallower* than predicted by the models, which lie on a relation with slope unity. The discrepancy in the re-

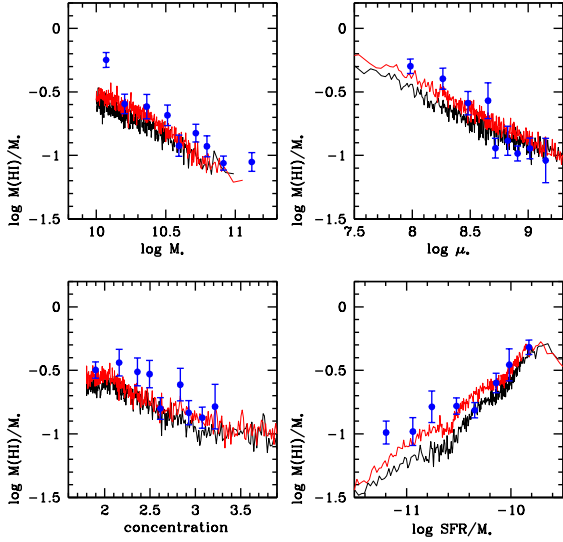


Figure 2. The mean HI mass fraction ($\log M(\text{HI})/M_*$) for COLD GASS galaxies with HI line detections (blue points) is plotted as a function of stellar mass, stellar mass surface density, concentration and specific star formation rate. Error bars are calculated using bootstrap resampling. Results for the F10 models are shown as black (KMT atomic-to-molecular gas prescription) and red (BR pressure prescription) curves.

lation between $M(\text{H}_2)/M_*$ and SFR/M_* is easily understood in light of the results presented in Saintonge et al (2011b). The F10 models adopt the assumption that $\Sigma_{\text{SFR}} = \alpha \Sigma_{\text{H}_2}$ with α constant (corresponding to an effective molecular gas depletion timescale of 2 Gyr) in all galaxies. This assumption was motivated by the results in Leroy et al (2008). Saintonge et al (2011) showed, however, that there was more than a factor of 5 variation in the *global* molecular gas depletion timescale in different galaxies, and that the least actively star-forming galaxies (i.e. lowest values of SFR/M_*) had the longest depletion times. This explains the shallow observed relation in the bottom right panel of Figure 3.

In Figure 4, we show scatter plots of $\log \text{SFR}/M_*$ versus $\log M(\text{H}_2)/M_*$ and $\log M(\text{HI})/M_*$ for our survey galaxies (blue points) and for galaxies from our mock catalogue (black points). Results are only shown for the KMT atomic-to-molecular gas prescription, because results for the pressure prescription are virtually the same. As can be seen the models reproduce the scatter in specific star formation rate versus atomic gas fraction quite well, but not in specific star formation rate versus molecular gas fraction. Clearly, there are additional processes at work that determine the rate at which molecular gas will form stars. This is the subject of a future paper (Saintonge et al, in preparation).

As well as looking at mean HI and H_2 mass fraction relations for galaxies with detections, it is instructive to analyze *full distribution functions* of gas mass fractions. These are illustrated in Figures 5 and 6. The data are shown as blue histograms, with error bars computed from bootstrap resampling. Black and red curves are for the models, as before. We plot distributions of $\log M(\text{HI})/M_*$ and $\log M(\text{H}_2)/M_*$ in three different intervals of stellar mass, stellar mass surface density and concentration. These plots show that the models

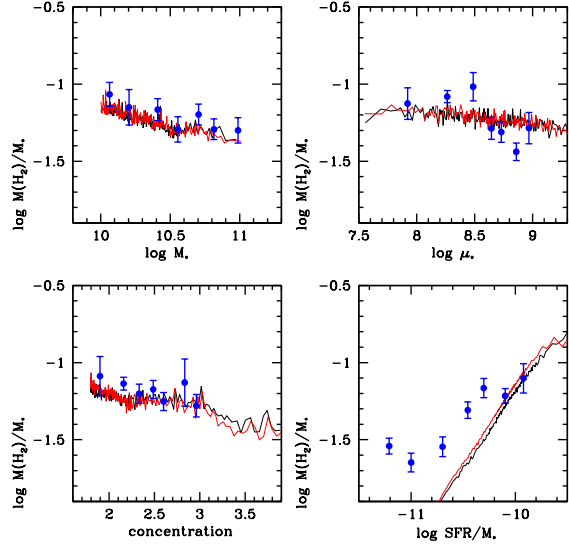


Figure 3. The mean H_2 mass fraction ($\log M(\text{H}_2)/M_*$) for COLD GASS galaxies with CO line detections (blue points) is plotted as a function of stellar mass, stellar mass surface density, concentration and specific star formation rate. Error bars are calculated using bootstrap resampling. Results for the F10 models are shown as black (KMT atomic-to-molecular gas prescription) and red (BR pressure prescription) curves.

provide a good representation not only of the mean HI/ H_2 mass fractions, but also of the *scatter around the mean*. As discussed in F10 and will be illustrated below, there is a tight relation between stellar mass and dark matter halo mass in the models. The scatter around the mean gas fraction at fixed dark matter halo mass is set by a) the spin parameter of the halo, which determines the contraction factor of the accreted gas and hence the rate at which it will be consumed into stars, and b) the recent gas accretion history of the galaxy. The fact that the scatter in the models and data agree so well lends support to this basic picture.

We note that in recent years, there have been a number of papers questioning the treatment of disk formation in semi-analytic models (e.g. Sales et al 2009). The primary objection is the assumption that the angular momentum of a galaxy expressed in units of that of its surrounding halo ($j_d = J_{\text{gal}}/J_{\text{vir}}$), correlates with mass of the galaxy divided by the mass of its dark matter halo ($m_d = M_{\text{gal}}/M_{\text{vir}}$) in a manner that is insensitive to feedback, i.e. $j_d = m_d$ is assumed for all halos. In our scheme this is *not* the case. We only assume that $j_d = m_d$ for the gas that is cooling instantaneously at any given time in any given halo. Because we track the growth of galaxies and dark matter halos with time, and because feedback effects will affect the mass of gas that cools in halos of different masses at different redshifts, the resulting relation between the angular momentum of the galaxy and its mass fraction will depend on feedback.

Figure 5 also shows that the models miss a minority population of galaxies with high atomic gas fractions and with low stellar masses, surface mass densities and concentrations. What are these missing galaxies? In three recent papers, we have studied the properties of galaxies in our survey that contain significantly more atomic gas than would

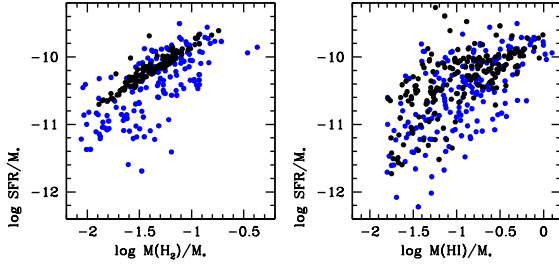


Figure 4. Scatter plots of H_2 mass fraction ($\log M(H_2)/M_*$, left) and HI mass fraction ($\log M(HI)/M_*$, right) for COLD GASS galaxies are shown as blue points. Results from the F10 models with KMT atomic-to-molecular gas prescription are shown as black points.

be predicted from their UV/optical colours and sizes (Moran et al 2010; Wang et al 2011; Moran et al 2011). The main conclusion is that such galaxies have very blue outer disks with young stellar populations and low gas-phase metallicities. These results led us to propose that these unusually HI-rich systems have experienced a recent gas accretion event, resulting in growth of the outer disk.

In the F10 models, the accreted gas is always added to the disk with an exponential surface density profile. In real galaxies, the accreted gas may initially be distributed in the outer regions of the galaxy. Dynamical perturbations in the form of spiral density waves, interaction with companions or with the non-axisymmetric gravitational potential of the surrounding dark matter halo, will eventually cause the gas to flow inwards and reach high enough densities to form molecular clouds. If we change the gas accretion prescriptions so that accreted gas is initially dumped in the outskirts of the disk, this may produce a tail of HI-rich galaxies. Observations of SFR, metallicity and gas profiles will be required to constrain models of this nature.

3.2 The nature of the quenched population

In this section, we investigate whether the “transition” between the population of galaxies with detectable atomic and molecular gas and the populations with gas fractions below ~ 0.015 occurs in the same way in models as in the data. In Figures 7 and 8, we plot the fraction of HI/CO-detected galaxies as a function of stellar mass, stellar mass surface density, concentration index and specific star formation rate. Results from the survey are shown as solid blue lines. The dashed blue lines indicate the $\pm 1\sigma$ uncertainty in the detected fraction as a function of these parameters. Models results are shown in red and black (the colour-coding is the same as in Figures 2 and 3). The main conclusion from these two figures is that the models and the data do not agree. First, the dependence of the detected fraction on stellar mass is weaker in the data than in the models. This is true for both the HI and the CO-detected fractions. Second, the fraction of CO-detected galaxies drops very strongly as a function of both stellar surface density and concentration in the real data. This is not seen in the models.

It is also instructive to look at the distribution of detected and non-detected galaxies in two-dimensional planes

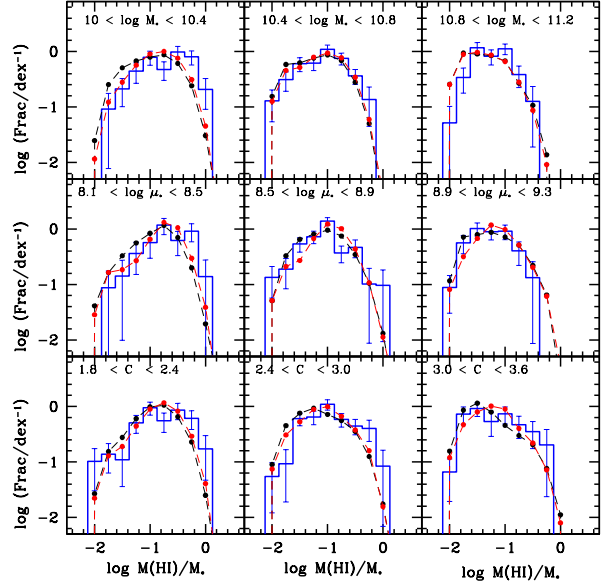


Figure 5. Distribution functions of HI mass fraction ($\log M(HI)/M_*$) for COLD GASS galaxies with HI line detections in 3 ranges of stellar mass, stellar mass surface density and concentration (blue histograms). Error bars are calculated using bootstrap resampling. Results for the F10 models are shown as black and red curves. The colour-coding of the model curves has the same meaning as in Figures 2 and 3.

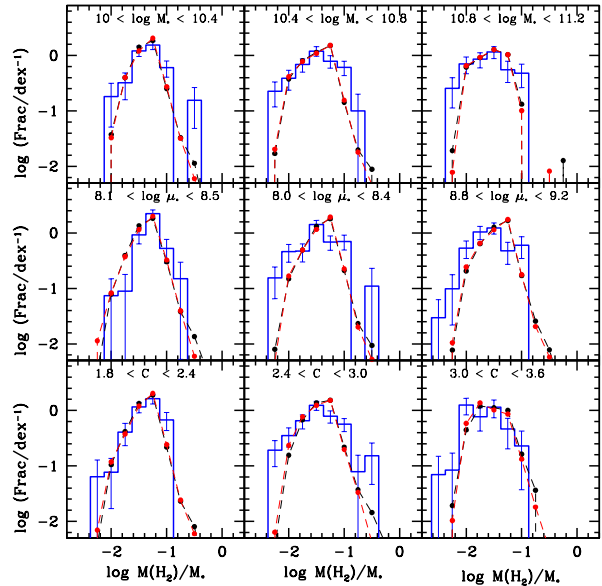


Figure 6. Distribution functions of H_2 mass fraction ($\log M(H_2)/M_*$) for COLD GASS galaxies with CO line detections in 3 ranges of stellar mass, stellar mass surface density and concentration (blue histograms). Error bars are calculated using bootstrap resampling. Results for the F10 models are shown as black and red curves. The colour-coding of the model curves has the same meaning as in Figures 2 and 3.

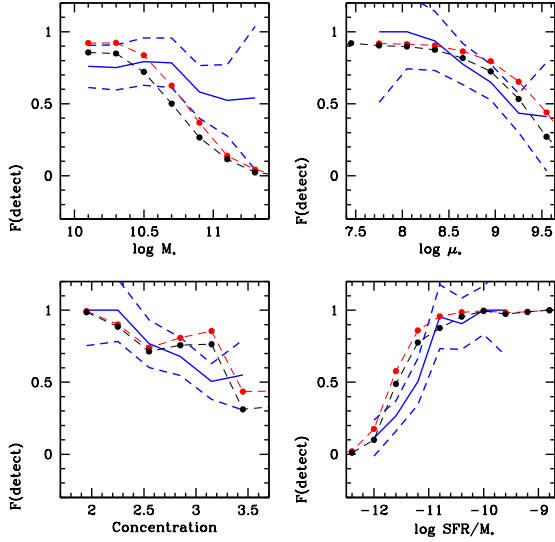


Figure 7. The fraction of COLD GASS galaxies with HI line detections is plotted as a function of stellar mass, stellar mass surface density, concentration and specific star formation rate (blue curve). Poisson errors are shown as blue dashed lines. We note that these are computed for independent bins, so the 1σ errors can be read off directly. Results for the F10 models are shown as black (KMT atomic-to-molecular gas prescription) and red (BR pressure prescription) curves.

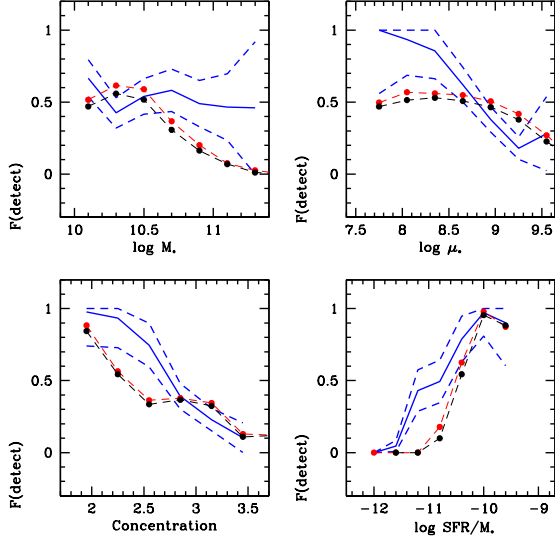


Figure 8. The fraction of COLD GASS galaxies with CO line detections is plotted as a function of stellar mass, stellar mass surface density, concentration and specific star formation rate (blue curve). Poisson errors are shown as blue dashed lines. Results for the F10 models are shown as black (KMT atomic-to-molecular gas prescription) and red (BR pressure prescription) curves.

of stellar mass and galaxy structural parameters. This is illustrated in Figures 9 and 10. We plot HI/CO detected galaxies in blue and HI/CO non-detected galaxies in red in the stellar surface density versus stellar mass, concentration versus stellar mass, and concentration versus stellar surface density planes. Results from the survey are shown in the top panels and results for “mock catalogues” of the same size generated from the simulations are shown in the bottom panels. In the data, there are clear *thresholds* in both μ_* ($\sim 3 \times 10^8 M_\odot \text{ kpc}^{-2}$) and C (~ 2.6), that demarcate the location of almost all galaxies without detectable gas. No such threshold is seen in stellar mass M_* . This is true for *both* the HI and the CO non-detections.

In the models, the parameters that most clearly demarcates the location of the HI non-detections are stellar mass surface density and stellar mass. It is the behaviour of the CO non-detections, however, that is most discrepant with the models. *Galaxies without H_2 are not confined to a specific location in structural parameter space in the same way as in the data.*

We also note that the tight correlation between stellar surface density and concentration index seen in the top right panels of both figures, is not present in the models. In addition, the distribution of concentration indices in the models extends to much lower values than in the real data. The tight correlation between C and $\log \mu_*$ tells us that in the real Universe, galaxies with larger bulge-to-disk ratios have disks with higher stellar surface densities.

In the F10 models, the effects of gas inflows on the disk are not taken into account, which may explain why there is no clear relation between bulge-to-disk ratio and stellar surface density. In a scenario where bulges form when gas flows inwards as a result of bar-driven inflows or other dynamical instabilities, the gas flows will not only form the bulge, but also increase the stellar surface mass density in the inner disk.

3.2.1 Origin of quenching thresholds in the models

We now elucidate the origin of the strong trend in the fraction of quenched galaxies as a function of stellar mass that is seen for the model galaxies. In current semi-analytic models, there are two physical processes that remove the supply of new gas to a galaxy and shut down star formation.

(i) *Radio Mode Feedback.* Black holes are able to grow by accreting hot gas from the surrounding halo. The growth rate is given by $\dot{M}_{\text{BH}} = \kappa(f_{\text{hot}}/0.1)(V_{\text{vir}}/200\text{km/s})^3(M_{\text{BH}}/10^8 M_\odot)M_\odot/\text{yr}$ (Croton et al 2006; Guo et al 2011), where f_{hot} is the ratio of hot gas mass to dark matter mass in the surrounding halo or sub-halo, V_{vir} is the virial velocity of the halo, M_{BH} is the black hole mass, and κ is an efficiency parameter. Some fraction of the rest mass energy of the accreted material is assumed to be transferred to the surrounding hot gas by radio jets. The models assume an energy input rate $\dot{E}_{\text{radio}} = 0.1\dot{M}_{\text{BH}}c^2$, where c is the speed of light. This leads to a reduction in the cooling rate of hot gas of the form $\dot{M}_{\text{cool,eff}} = \dot{M}_{\text{cool}} - 2\dot{E}_{\text{radio}}/V_{\text{vir}}^2$.

(ii) *Gas stripping.* When a galaxy is accreted by a more massive dark matter halo, it becomes a “satellite”. In the models of De Lucia & Blaizot (2007), the hot gas surround-

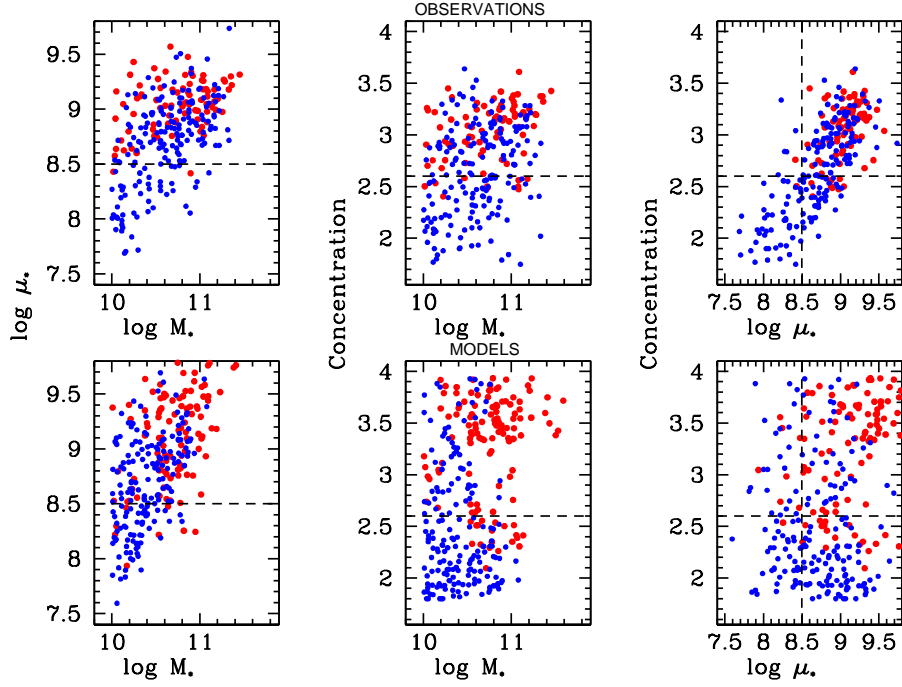


Figure 9. Top: COLD GASS galaxies are plotted in the 2-dimensional planes of stellar surface density versus stellar mass, concentration versus stellar mass and concentration versus stellar surface density. Galaxies with HI line detections are plotted in blue, while those without HI line detections are plotted in red. Bottom: Detections and non-detections from our F10 model “mock catalogues” are plotted in the same 3 planes.

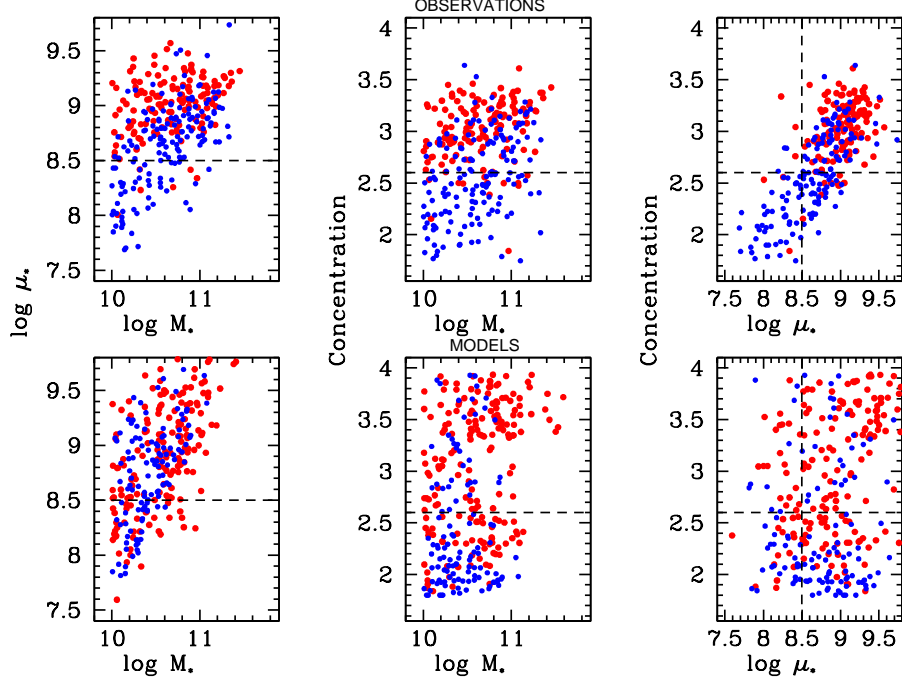


Figure 10. Top: COLD GASS galaxies are plotted in the 2-dimensional planes of stellar surface density versus stellar mass, concentration versus stellar mass and concentration versus stellar surface density. Galaxies with CO line detections are plotted in blue, while those without CO line detections are plotted in red. Bottom: Detections and non-detections from our F10 model “mock catalogues” are plotted in the same 3 planes.

ing the satellite is stripped instantaneously, leading to a sharp reduction in the cooling rate onto the satellite. In the more recent models of Guo et al (2011), the dark matter and hot gas surrounding the satellite are removed more gradually both by tidal forces and by ram-pressure stripping.

The parameter κ is tuned to reproduce the high mass end of the stellar mass function. The net effect is illustrated in Figure 11 where we plot galaxies from our model catalogue in the 2D planes of subhalo mass versus $\log M_*$, subhalo mass versus $\log \mu_*$, and subhalo mass versus C . Galaxies that are predicted to be detected in CO are colour-coded blue, while those predicted to be non-detections are colour-coded red. Figure 11 shows a clear transition between active and quenched galaxies at a subhalo mass of $10^{12} M_\odot$, which is a factor of ~ 3 larger than the mass where dark matter halos are predicted to transition to hosting a static halo of hot gas (Birnboim & Dekel 2003; Dekel & Birnboim 2006; Croton et al 2006). The reason why the transition is very sharp in halo mass is because the primary dependence of the mass that is accreted by the black hole is on halo virial velocity and not on black hole mass. We note that there is an additional population of quenched galaxies in low mass subhalos. These are the satellite galaxies, where the subhalo has been stripped by tidal forces. As can be seen, they form a small minority of the quenched population in the stellar mass range of the galaxies in the GASS survey.

Figure 11 clearly illustrates *why* quenching in the model galaxies is most strongly dependent on stellar mass and surface density, and largely independent of concentration. This is because in the model, stellar mass and surface density correlate with the virial mass of the host halo, but concentration does not. There is direct observational evidence in support of these results. Mandelbaum et al (2006) used weak gravitational lensing to derive halo masses of galaxies as a function of stellar mass and morphology. They found stellar mass to be a good proxy for halo mass. For a given halo mass, the stellar mass was independent of concentration/morphology below $M_* = 10^{11} M_\odot$.

3.2.2 Origin of quenching thresholds in real galaxies

In the data, quenching thresholds are seen as a function of stellar surface density and concentration, but not as a function of stellar mass. Even for galaxies with stellar masses as high as $10^{11} M_\odot$, which are observed to reside in halos with masses in the range $3 \times 10^{12} - 10^{13} M_\odot$, HI and CO are generally still detected if concentrations and densities are low. This strongly suggests that *processes associated with bulge formation must be responsible for shutting off the gas supply in galaxies*.

We note that this hypothesis was already put forward by Kauffmann et al (2006), based on an analysis of the *scatter* in the colours and spectral properties of galaxies as a function of stellar mass, stellar surface density and concentration. Kauffmann et al (2006) made an ansatz that scatter in specific star formation rate reflected scatter in gas content. The fact that specific star formation rates as well as their scatter decreased sharply above a characteristic density threshold of $3 \times 10^8 M_\odot \text{ kpc}^{-2}$ and concentration index of 2.6 and that this threshold was largely independent of the stellar mass of the galaxy, was taken as evidence that gas accretion

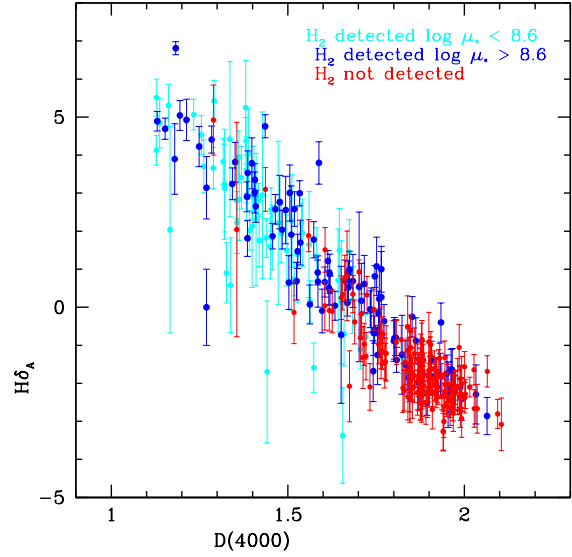


Figure 12. The Lick $H\delta_A$ index is plotted as a function of 4000 Å break strength for COLD GASS with CO line detections and $\log \mu_* > 8.6$ (blue). CO line detections and $\log \mu_* < 8.6$ (cyan) and for COLD GASS galaxies with no CO line detections (red). The errors on each measurement are also indicated for each galaxy.

was no longer occurring in bulge-dominated systems. The COLD GASS and GASS surveys have now demonstrated that the neutral gas content of galaxies is weakly dependent on stellar mass and decreases sharply at $\mu_* > 3 \times 10^8 M_\odot \text{ kpc}^{-2}$ and $C > 2.6$.

We have not yet ascertained *why* bulge-dominated galaxies no longer accrete gas and form stars efficiently. Figure 3 shows that galaxies with $\mu_* > 3 \times 10^8 M_\odot \text{ kpc}^{-2}$ have molecular gas mass fractions that are slightly depressed relative to model predictions. Could such galaxies be transitioning to the red sequence on short timescales as proposed by Schawinski et al (2009)?

We note that molecular gas is generally concentrated towards the inner regions of galaxies. The SDSS fiber spectra probe the central 1-2 kpc central regions of the GASS galaxies and contain diagnostics of the recent star formation history in the bulge. In Figure 12, we plot $H\delta_A$ as a function of $D_n(4000)$ for the galaxies in the survey. Galaxies where CO was not detected are colour coded red, those with detections and $\log \mu_* > 8.6$ are colour coded-blue, and those with detections and $\log \mu_* < 8.6$ are colour-coded cyan. As discussed in detail in Kauffmann et al (2003a), by combining these two stellar absorption line indices, we can diagnose if the recent star formation histories of a population of galaxies have been smooth or “bursty” on average. Starbursts of duration less than 1-2 hundred million years, displace a significant fraction of galaxies to higher values of $H\delta_A$ at a given value of $D_n(4000)$. Likewise, if star formation is truncated over a timescale of less than a few hundred million years, galaxies will also be displaced to higher than average values of $H\delta_A$ for around a Gyr following the truncation event (see for example, Kauffmann et al 2004).

As can be seen, most GASS galaxies lie on the same locus in the plane of $H\delta_A$ versus $D_n(4000)$. There is no ev-

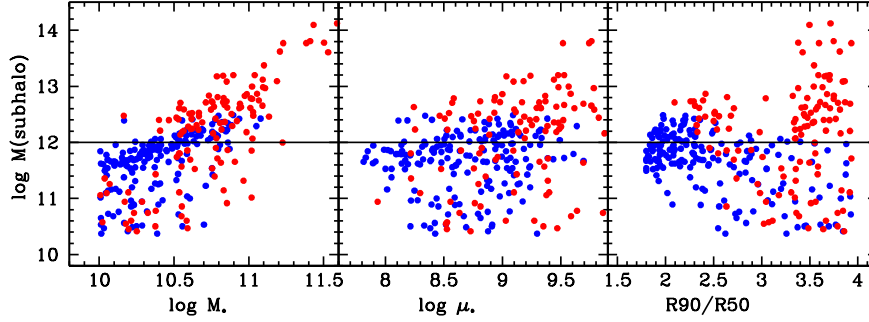


Figure 11. F10 model galaxies are plotted in the 2-dimensional planes of subhalo mass versus stellar mass, subhalo mass versus stellar surface density and subhalo mass versus concentration. Galaxies predicted to have CO line detections are plotted in blue, while those predicted not to have CO line detections are plotted in red.

idence of any net displacement as a function of stellar surface density or as a function of H_2 mass fraction, indicating that the star formation histories of most high surface density galaxies with gas have been smooth. We note, however, that galaxies with CO line detections and high stellar surface densities *do span the largest range in stellar population parameters*. They have $D_n(4000)$ values as low as those of the low-density H_2 -rich population, and as high as those of the “quenched” population. We also note that the three post-starburst galaxies that are clearly displaced to higher values of $H\delta_A$, are all detected in H_2 and have high stellar surface densities. All of them have unusually high molecular-to-atomic gas ratios, and one is clearly the end product of a recent merger (tidal features are visible in the SDSS image).

This region of parameter space is clearly quite complex, and may consist of several distinct sub-populations of galaxies on different evolutionary trajectories. If so, additional data will be required to pull these apart. In particular, studies of the *distribution and the kinematics of the gas* may shed significant light on its origin and its eventual fate.

4 SUMMARY

We compare the semi-analytic models of galaxy formation of Fu et al. (2010), which track the evolution of atomic and molecular gas in galaxies, with gas fraction scaling relations derived from a stellar mass-limited sample of 299 galaxies from the COLD GASS survey. These galaxies have measurements of the CO(1-0) line from the IRAM 30-m telescope and the HI line from Arecibo, as well as measurements of stellar masses, structural parameters and star formation rates derived from GALEX+SDSS photometry.

Our analysis addresses two key questions: 1) Can the semi-analytic disk formation models explain the observed gas fraction scaling relations in galaxies with gas and ongoing star formation?, 2) Does the transition between the population of galaxies with gas and the “quenched” population without gas occur in the same way in the models and in the data?

In answer to the first question, we conclude that the disk models provide a reasonable description of how condensed baryons are partitioned into stars, atomic gas and molecular gas as a function of galaxy mass and size. Trends

as a function of bulge-to-disk ratio are not well reproduced. In particular, the models do not account for the fact that at fixed stellar mass, there is a tight relation between the size of a galaxy and its bulge-to-disk ratio.

In answer to the second question, we conclude that our data disagree with the current *implementation* of radio-mode feedback in the models. In the models, the observable parameter that best predicts whether a galaxy has been quenched is its stellar mass. Our data shows that the fraction of quenched galaxies is largely independent of stellar mass, but depends strongly on galaxy bulge-to-disk ratio and stellar surface density. In other words, even low mass galaxies with bulges have high probability of being quenched. We conclude that processes associated with bulge formation are thus likely to be responsible both for depleting the neutral gas in galaxies and for shutting off the gas supply in these systems.

Solving these problems will require substantive changes to the way gas transport and bulge and black hole formation is treated in the models, as well as to the way feedback from AGN is implemented. We now outline our best guess as to how this might work in practice.

In the current models, newly accreted gas is assumed to have an exponential profile. If the profile is initially shallower than exponential, more atomic gas would collect in a largely inert reservoir in the outer regions of the galaxy. This gas would later be driven towards the center of the galaxy by dynamical perturbations, where it would form molecular gas and stars in the inner region of the disk. The inflowing gas would also contribute to the growth of the bulge. A prescription of this kind may result in a better correlation between stellar surface mass density and bulge-to-disk ratio.

There is now evidence from studies of complete samples of nearby galaxies that bars are very common in disk galaxies. Barazza, Jogee & Marinova (2008) find that 70% of disk-dominated galaxies host bars. Moreover, barred galaxies (in particular galaxies with strong bars) are associated with higher central molecular gas fractions and enhanced rates of central star formation (Sakamoto et al 1999; Ellison et al 2011; Wang et al 2012, in preparation), suggesting that bulges are forming in these systems. Finally, barred galaxies do not exhibit any excess of nearby companions, suggesting that they are not triggered by interactions (Li et al. 2009).

All of this suggests that internally-driven gas transport

processes are important in the formation of bulges, but resolved maps of the atomic and molecular gas distributions in complete samples of galaxies and more detailed theoretical calculation of gas inflow rates in galaxies are required in order to quantify this in more detail.

In the current models, radio-mode feedback suppresses the cooling of gas in halos more massive than $10^{12} M_{\odot}$. In addition, in massive, high density galaxies, atomic gas is transformed very efficiently into molecular gas and thence into stars. These two mechanisms appear to be sufficient to place all “HI-quenched” galaxies in the high M_* and μ_* corner of parameter space, as seen in the bottom panel of Figure 9. The same mechanisms are not, however, sufficient to place the “H₂-quenched” galaxies in this same region of parameter space. Nor can they explain why galaxies deficient in both HI and H₂ are almost always found in galaxies with substantial bulge components. The simplest inference is that the neutral gas in galaxies is either consumed or removed when bulges form, and that subsequent gas accretion into the atomic phase is suppressed in a significant fraction of bulge-dominated galaxies.

More detailed studies of the spatially-resolved kinematics of the gas and how gas motions across galaxies correlate with the presence of accreting black holes, jets and the distribution of star formation, will be needed before we are able to pinpoint the actual physical mechanisms responsible for removing/depleting the gas in these systems (see for example Hopkins et al 2011). Quenching may occur over short timescales during particular phases of bulge formation, so it may be necessary to survey large samples before a definitive conclusion can be reached. In addition, the mechanisms that inhibit the late accretion of gas in bulge-dominated systems remain to be clarified.

ACKNOWLEDGMENTS

This work is based on observations carried out with the IRAM 30 m telescope. IRAM is supported by INSU/CNRS (France), MPG (Germany), and IGN (Spain). We sincerely thank the staff of the telescope for their help in conducting the COLD GASS observations and Qi Guo for helpful discussions.

REFERENCES

- Baldry I. K., Glazebrook K., Brinkmann J., Ivezić Ž., Lupton R. H., Nichol R. C., Szalay A. S., 2004, *ApJ*, 600, 681
- Barazza F. D., Jogee S., Marinova I., 2008, *ApJ*, 675, 1194
- Bigiel F., Leroy A., Walter F., Brinks E., de Blok W. J. G., Madore B., Thornley M. D., 2008, *AJ*, 136, 2846
- Blitz L., Rosolowsky E., 2006, *ApJ*, 650, 933 (BR)
- Bower R. G., Benson A. J., Malbon R., Helly J. C., Frenk C. S., Baugh C. M., Cole S., Lacey C. G., 2006, *MNRAS*, 370, 645
- Catinella B., et al., 2010, *MNRAS*, 403, 683
- Cattaneo A., Dekel A., Devriendt J., Guiderdoni B., Blaizot J., 2006, *MNRAS*, 370, 1651
- Croton D. J., et al., 2006, *MNRAS*, 365, 11
- De Lucia G., Kauffmann G., White S. D. M., 2004, *MNRAS*, 349, 1101
- De Lucia G., Blaizot J., 2007, *MNRAS*, 375, 2
- Dutton A. A., van den Bosch F. C., Dekel A., 2010, *MNRAS*, 405, 1690
- Ellison S. L., Nair P., Patton D. R., Scudder J. M., Mendel J. T., Simard L., 2011, *MNRAS*, 416, 2182
- Fu J., Guo Q., Kauffmann G., Krumholz M. R., 2010, *MNRAS*, 409, 515 (F10)
- Gnedin N. Y., Tassis K., Kravtsov A. V., 2009, *ApJ*, 697, 55
- Governato F., et al., 2004, *ApJ*, 607, 688
- Governato F., Willman B., Mayer L., Brooks A., Stinson G., Valenzuela O., Wadsley J., Quinn T., 2007, *MNRAS*, 374, 1479
- Guo Q., et al., 2011, *MNRAS*, 413, 101
- Hopkins P. F., Quataert E., Murray N., 2011, *arXiv*, arXiv:1110.4638
- Kauffmann G., et al., 2003, *MNRAS*, 341, 33
- Kauffmann G., et al., 2003, *MNRAS*, 341, 54
- Kauffmann G., White S. D. M., Heckman T. M., Ménard B., Brinchmann J., Charlot S., Tremonti C., Brinkmann J., 2004, *MNRAS*, 353, 713
- Kauffmann G., Heckman T. M., De Lucia G., Brinchmann J., Charlot S., Tremonti C., White S. D. M., Brinkmann J., 2006, *MNRAS*, 367, 1394
- Keres D., Yun M. S., Young J. S., 2003, *ApJ*, 582, 659
- Krumholz M. R., McKee C. F., Tumlinson J., 2009, *ApJ*, 693, 216 (KMT)
- Lagos C. D. P., Lacey C. G., Baugh C. M., Bower R. G., Benson A. J., 2011, *MNRAS*, 416, 1566
- Leroy A. K., Walter F., Brinks E., Bigiel F., de Blok W. J. G., Madore B., Thornley M. D., 2008, *AJ*, 136, 2782
- Li C., Gadotti D. A., Mao S., Kauffmann G., 2009, *MNRAS*, 397, 726
- Lu Y., Mo H. J., Weinberg M. D., Katz N., 2011, *MNRAS*, 416, 1949
- Malbon R. K., Baugh C. M., Frenk C. S., Lacey C. G., 2007, *MNRAS*, 382, 1394
- McNamara B. R., Nulsen P. E. J., 2007, *ARA&A*, 45, 117
- Mo H. J., Mao S., White S. D. M., 1998, *MNRAS*, 295, 319
- Moran S. M., et al., 2010, *ApJ*, 720, 1126
- Moran S. M., et al., 2011, *arXiv*, arXiv:1112.1084
- Navarro J. F., Steinmetz M., 1997, *ApJ*, 478, 13
- Obreschkow D., Croton D., De Lucia G., Khochfar S., Rawlings S., 2009, *ApJ*, 698, 1467
- Oser L., Ostriker J. P., Naab T., Johansson P. H., Burkert A., 2010, *ApJ*, 725, 2312
- Robertson B. E., Kravtsov A. V., 2008, *ApJ*, 680, 1083
- Saintonge A., et al., 2011a, *MNRAS*, 415, 61
- Saintonge A., et al., 2011b, *MNRAS*, 415, 32
- Sakamoto K., Okumura S. K., Ishizuki S., Scoville N. Z., 1999, *ApJ*, 525, 691
- Sales L. V., Navarro J. F., Schaye J., Dalla Vecchia C., Springel V., Haas M. R., Helmi A., 2009, *MNRAS*, 399, L64
- Schawinski K., et al., 2009, *ApJ*, 690, 1672
- Schiminovich D., et al., 2010, *MNRAS*, 408, 919
- Somerville R. S., Hopkins P. F., Cox T. J., Robertson B. E., Hernquist L., 2008, *MNRAS*, 391, 481
- Strateva I., et al., 2001, *AJ*, 122, 1861

- Wang J., et al., 2011, MNRAS, 412, 1081
Weinmann S. M., Kauffmann G., van den Bosch F. C.,
Pasquali A., McIntosh D. H., Mo H., Yang X., Guo Y.,
2009, MNRAS, 394, 1213
Williams R. J., Quadri R. F., Franx M., van Dokkum P.,
Toft S., Kriek M., Labbé I., 2010, ApJ, 713, 738
Wuyts S., et al., 2011, arXiv, arXiv:1107.0317
Young J. S., et al., 1995, ApJS, 98, 219